Check for updates

Performances of Concrete Columns with Modular UHPC Permanent Formworks Under Axial Load

Yibo Yang[1,2], Baixi Chen[3*] , Yong Chen[2], Huanyang Zhou[2], Fucai Liu[4], Xiangming Xie[5], Junsheng Chen[1,2], Wenying Guo[2] and Hengchang Wang[2]

Abstract

This research proposed the modular prefabricated permanent formwork system made of ultra-high-performance concrete (UHPC). Two kinds of modular formwork shapes were designed: the flat formwork and the ribbed. The experimental investigation on the axial compression performance of the composite columns that consist of the normal strength concrete (NSC) core and the modular UHPC permanent formwork was demonstrated. Compared with the flat formwork, the ribbed formwork exhibited better bonding with the NSC core. As observed from the test results, the composite column with the ribbed formwork presented a similar axial behavior as the NSC column with a slight improvement in ultimate loads. Therefore, the modular UHPC ribbed permanent formwork could be regarded as the additional cover to the conventional NSC column. In addition, the finite element analysis (FEA) model was also developed to simulate the composite columns numerically. The predicted capacities agreed with the experimental results, which validated the numerical models. The crack pattern estimated by the FEA model revealed that the interaction between the permanent formwork and the inner concrete introduced many tiny cracks to the concrete core. However, as protected by the UHPC permanent formwork, the overall durability of the composite columns can still be enhanced.

Keywords Modular permanent formwork, Ultra-high-performance concrete (UHPC), Composite column, Axial compression performance

1 Introduction

Concrete is widely used and investigated in the current building development (Jiang & Shen, 2022; Jiang et al., 2021; Li et al., 2022a; Yang et al., 2018, 2021). The formwork construction is an inevitable step in constructing cast-in-situ concrete structures. The conventional formwork system requires the setup and the dismantlement, which is both time and labor-intensive. According to the previous estimations (Jha, 2012; Robert, 2007), the labor cost of conventional formwork systems takes up more than 50% of the total cost of a new concrete construction project. As an alternative to traditional formwork systems, the prefabricated permanent formwork system has exhibited a dramatic capacity in recent years. The permanent formwork system could reduce both the on-site

Yang *et al. Int J Concr Struct Mater*   (2023) 17:38

Page 2 of 14

construction labor cost and time by eliminating the step of dismantling the formworks (Remy et al., 2011). Since the permanent formworks remain in place after the casting, they could also work as external jackets to protect the inner concrete from environmental attacks.

There were various types of permanent formworks developed in the existing studies. Several researchers (Chahrour & Soudki, 2006; Fakharifar & Chen, 2016; Kildashti et al., 2020; Kuder et al., 2009) employed polyvinyl chloride (PVC) as an economical and durable permanent formwork. The axial performance of the concrete columns encased by the PVC permanent formwork was experimentally and numerically investigated by Kildashti et al. (2020). Moreover, Chahrour and Soudki (2006) also provided a theoretical model to estimate the axial capacity of the PVC-encased column. Considering the high strength-to-weight ratio, some scholars (Ozbakkaloglu & Saatcioglu, 2007; Tian et al., 2019; Ying et al., 2021; Zhang et al., 2015) used the fiber-reinforced polymer (FRP) casings as the permanent formworks for the concrete column. The axial performances of the square and circular concrete columns fabricated by the FRP permanent formworks were experimentally studied by Ozbakkaloglu et al. (2007) and Zhang et al. (2015), respectively. The FRP formwork could enhance the strength and ductility of the inner concrete, but it is vulnerable to high temperatures (Hu et al., 2018). The steel tube is another popularly used permanent formwork for columns (Cai et al., 2019; Ghanbari-Ghazijahani et al., 2020). The concrete column with the steel tube showed better compression behaviors than the conventional concrete columns (Abed et al., 2013; Han et al., 2019; Wei et al., 2019). However, the fire-resistance issue is also faced by the steel tube formwork.

Ultra-high-performance concrete (UHPC) is an innovative cementitious material that has attracted many researchers in recent years. Previous studies (Azmee & Shafiq, 2018; Graybeal & Tanesi, 2007; Magureanu et al., 2012; Shafieifar et al., 2017; Shi et al., 2015) stated that the UHPC possesses ultra-high compressive strength, excellent durability, and high crack resistance due to its dense microstructure. Since the UHPC exhibits a superior strength-to-weight ratio over the conventional cement-based material, it is an excellent choice to use the UHPC for producing lightweight permanent formwork. As a cementitious material, the UHPC has a good fire-resistant capacity (Xiong & Liew, 2015; Ye et al., 2012), which makes the UHPC permanent formwork fire-proof. In addition, the excellent durability of the UHPC makes the formworks provide the inner concrete with sufficient protection and lower maintenance costs.

The promising advantages of the UHPC permanent formwork have drawn many scholars' attention (Fang et al., 2023; Hadi et al., 2018; Huang et al., 2021; Shan et al., 2018, 2020; Tian et al., 2020; Wu et al., 2018; Zeng et al., 2022; Zhang et al., 2022). Shan et al. (2018) prepared the tubular formwork using reactive powder concrete (RPC), one type of UHPC, for molding the concrete columns. The obtained concrete column with the RPC tube demonstrated higher load capacity and better corrosion resistance than the conventional concrete column. A similar conclusion was also drawn by Hadi et al. (2018). Tian et al. (2020) proposed a prefabricated grid-reinforced UHPC permanent formwork for the concrete column and investigated the column axial behavior experimentally and numerically. While the load-carrying capacity and elastic modulus were improved, the ductility of the composite column was decreased by the brittle nature of the UHPC. An FRP-reinforced UHPC tubular formwork was developed by Zeng et al. (2022), and the effects of the tube thickness and fiber addition were studied. The developed FRP-reinforced UHPC tubular formwork showed the capacity to strengthen the deteriorated columns. Huang et al. (2021) developed a composite permanent formwork system, where the UHPC worked as the exterior layers, and the engineered cementitious composite worked as the interior layers. The ordinary concrete filled the space between two layers. The composite formwork presented the desirable mechanical performance as well. In addition, a high strength cementitious grout was also developed by Yang et al. (2023a, b) to fill the joints existing in the UHPC permanent formworks and improve the formwork system's performances.

Although many UHPC permanent formwork systems were introduced in the previous works, most of them were prefabricated to the customized member geometry. In the construction project, there usually are plenty of different member geometries. Manufacturing a customized formwork for each structural member geometry not only adversely influences the production efficiency, but also raises the formwork cost (Li et al., 2022b). Therefore, the standardized modular UHPC permanent formwork system is proposed in this study to solve this issue. With the advantages of cement-based materials, the proposed modular UHPC formwork could cooperate with the casted concrete well and has better fire and corrosion resistance than other materials, like PVC and FRP, previously used as permanent formworks. In comparison with the previous one-piece UHPC formwork, the modular UHPC formwork is more versatile and flexible. Most member geometries could be erected quickly by assembling the modular formwork. With the standardized shape, the modularization of the UHPC permanent formwork system could speed up the production of prefabricated members and reduce manufacturing costs.

Yang *et al. Int J Concr Struct Mater*   (2023) 17:38

Page 3 of 14

Additionally, the modular UHPC permanent formwork can be interchanged with conventional modular formwork, making it easy to adopt on-site.

In the rest of the paper, the modular UHPC permanent formworks with the flat shape and the ribbed shape are described first, and then the experimental and numerical studies on the axial behavior of the concrete column fabricated by the modular UHPC permanent formworks are conducted.

2 Experimental Program

2.1 Design of Experiment

Two types of modular UHPC permanent formworks, namely the flat formwork and the ribbed formwork, were proposed in this paper. The geometries of two UHPC permanent formworks are illustrated in Fig. 1. The height (i.e., 400 mm) and width (i.e., 100 mm) of two permanent formworks are the common divisor of most column height and width, respectively. Therefore, the modular UHPC permanent formworks could be assembled to erect the whole permanent formwork systems for various geometries.

Since the integrity of the modular formwork system was not so strong, the UHPC modular permanent formwork was designed as the non-associated formwork, which only sustains the outward pressure developed by the concrete core (Kildashti et al., 2021). As the non-associated formwork, the UHPC modular permanent formworks have two main possible utilizations:

(1) The UHPC formworks were used as the replacement of the cover layer of the normal strength concrete (NSC), which did not influence the section size of the conventional concrete column.

(2) The UHPC formworks were regarded as the additional cover layer of the NSC, which increased the section size of the conventional concrete column.

In order to investigate which utilization was reasonable in reality, five kinds of column cross-sections were proposed here, and they are presented in Fig. 2. The ratio of the specimen scale in Fig. 2 to the real structure is 1/3. Columns A–C were the conventional concrete columns, while columns D and E were the composite columns with the UHPC flat permanent formworks and the UHPC ribbed permanent formworks, respectively. Similar to conventional formworks, the UHPC permanent formworks were attached to the cast-in-place concrete by the concrete adhesive force. Column A was used as the reference. Column B had the same concrete cover thickness as the composite columns. The comparison between column B and the composite columns was used to demonstrate if the UHPC modular permanent formworks could work as the replacement for the concrete cover. The cross-section size of column C was the same as the NSC concrete cores of the composite columns D, and E. Column C was employed to illustrate the effect of the UHPC modular formworks when the UHPC formworks worked as the additional concrete cover.

Considering the story height of 3.6 m and the scale ratio of 1/3, the height of the column specimens was set to 1200 mm. The schematic diagrams of the conventional concrete columns and the composite concrete columns are shown in Fig. 3a, b. The cast-in-place concrete was reinforced by the longitudinal bars of Φ 16 mm and the transverse bars of Φ 8 mm, while no reinforcement was used for the UHPC permanent formworks. The distributions of the longitudinal reinforcements and the stirrups in the cast-in-place concrete are presented in Figs. 2 and 3c, respectively. Two specimens were prepared for each column section (i.e., a totally 10 specimens), and the details of the specimens are presented in Table 1.
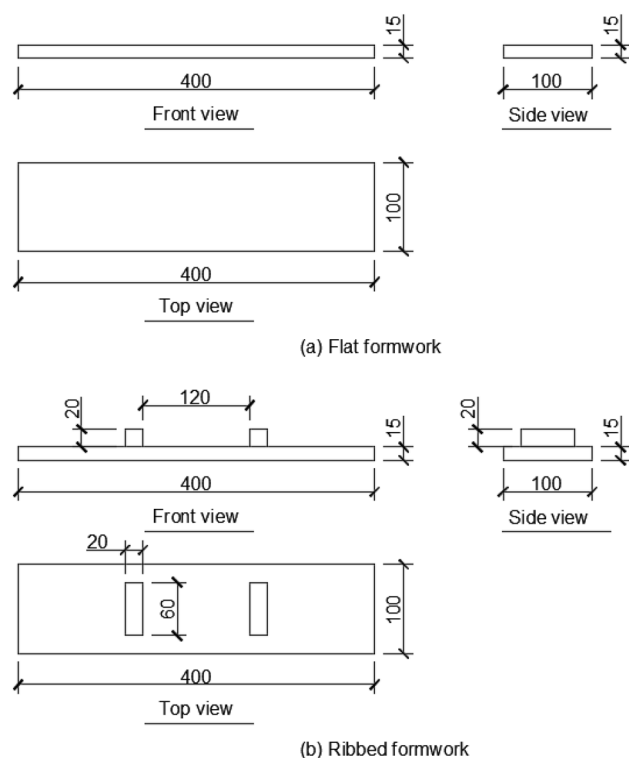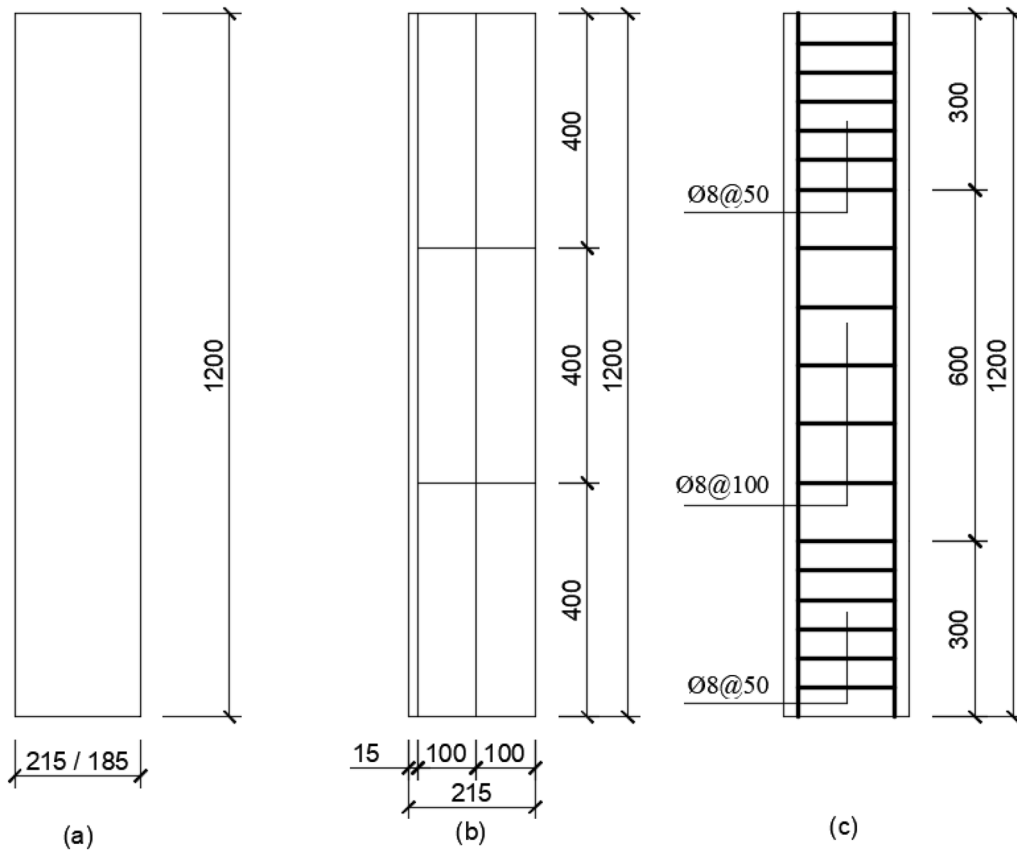

Fig. 1 The geometries of two UHPC permanent formworks: **a** flat formwork; **b** ribbed formwork (unit: mm)

2.2 Material Property

This research used the factory-produced UHPC dry mix to prepare the modular UHPC permanent formworks. The UHPC dry mix contained the aggregate and the binding
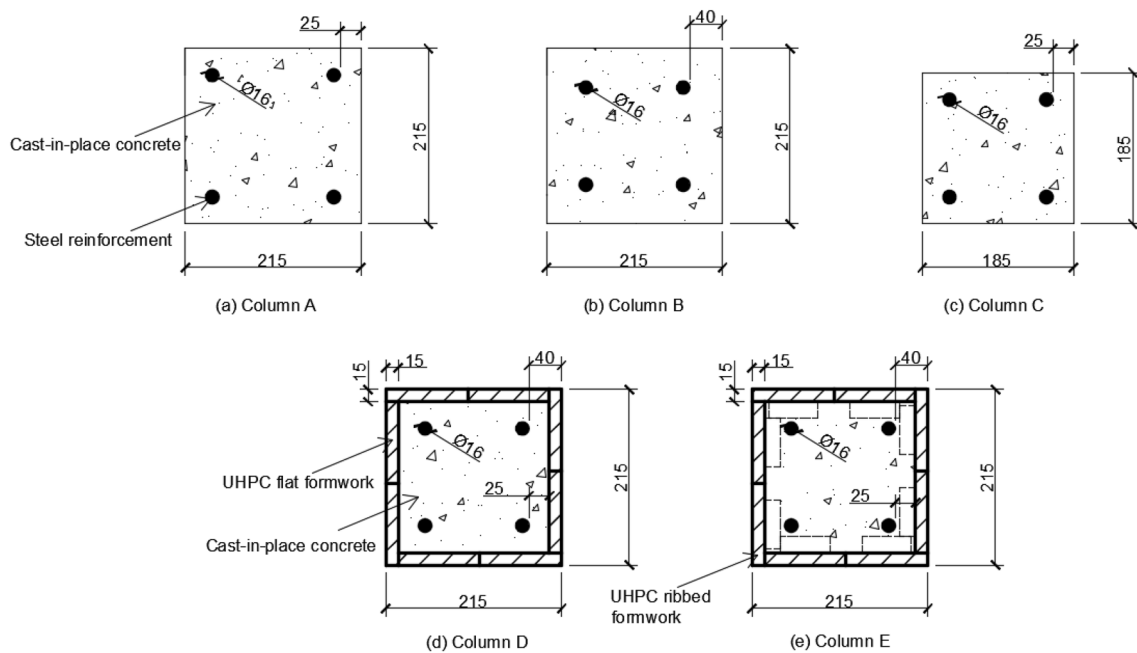
Fig. 2 Cross-sections of the concrete columns (unit: mm)

Fig. 3 The schematic diagrams of concrete columns. **a** The conventional concrete column. **b** The composite column with the UHPC permanent formworks, and (**c**) the reinforcements distributions of the columns (unit: mm)

Table 1 Details of the experimental specimens

Column types		Specimen	Section size (mm×mm)	Height (mm)	Concrete cover thickness[a] (mm)	Area of reinforcement[b] (mm²)	Reinforcement ratio (%)
Without UHPC formworks	A	A-1	215×215	1200	25	4 Φ 16 (804)	1.739
		A-2					
	B	B-1	215×215	1200	40	4 Φ 16 (804)	1.739
		B-2					
	C	C-1	185×185	1200	25	4 Φ 16 (804)	2.349
		C-2					
With UHPC formworks	D	D-1	215×215	1200	40	4 Φ 16 (804)	1.739
		D-2					
	E	E-1	215×215	1200	40	4 Φ 16 (804)	1.739
		E-2					

[a] Concrete cover thickness includes the thickness of the UHPC permanent formworks

[b] Longitudinal reinforcement

Table 2 Mixture proportion and compressive strength of the UHPC used to prepare the permanent formworks

	W/B ratio	Mixture proportion (kg/m³)			Compressive strength (MPa)
		UHPC dry mix	Water	Water reducer	
UHPC	0.16	2100	120.8	78.8	125

materials with a ratio of 1:1. The binding material was composed of cement, silica fume, slag powder, and fly ash with a proportion of 0.7:0.15:0.10:0.05. The aggregate size of the UHPC dry mix ranged from 0.15 mm to 1.18 mm. Based on the preliminary study on the UHPC, the water to binder (*W/B*) ratio was set to 0.16. And the water reducer with a solid content of 40% was employed here. The adopted mixture proportion is illustrated in Table 2. The compressive strength of the UHPC was tested according to Chinese Code JC/T 1004-2006 (2006). The concrete strength test and the column specimen tests were completed within two days to ensure that the concrete has the same strength. The measured 28 days compressive strength is presented in Table 2.

The mixture proportion of the cast-in-place NSC is demonstrated in Table 3. The cement used here was P.II 42.5R cement, and the river sand was the Zone II fine sand specified by the code GB/T 14684-2011 (2011). The coarse

aggregate A and B size ranges were 2.36–9.5 mm and 2.36–19.0 mm, respectively. The compressive strength of the NSC is also listed in Table 3. The yield strength, ultimate strength, and elastic modulus of the steel reinforcement were 411.82 MPa, 585 MPa, and 206 GPa, respectively.

2.3 Specimen Preparations

The UHPC permanent formworks were prefabricated by casting the fresh UHPC into the molds with the designed shapes. Before demolded, the UHPC permanent formworks were cured at room temperature (20 ± 2 ℃) for 6 h and then were cured at a temperature of 40 ± 5 ℃ for 18 h. The demolded UHPC formworks were cured in the steam curing room at a temperature of 90 ± 5 ℃ for 48 h. After the steam curing, the UHPC formworks were moved into the concrete standard curing room with a temperature of 20 ± 1 ℃ and an R.H. over 95% until use.

The conventional concrete columns (i.e., columns A, B, and C) were cast using the wood formworks, which were moved away after curing for one day. The composite columns (i.e., columns D and E) were cast using the UHPC permanent formwork systems, which stayed in place. All column specimens were covered by the cloth and cured at room temperature for 150 days before testing.

Table 3 Mixture proportion and compressive strength of the cast-in-place NSC

	W/B ratio	Mixture proportion (kg/m³)						Compressive strength (MPa)
		Water	Cement	River sand	Coarse aggregate A	Coarse aggregate B	Water reducer	
NSC	0.44	180.1	411.4	715	858.0	214.5	3.7	45.7 (for 28 days), 50.2 (for 150 days)

Yang *et al. Int J Concr Struct Mater*   (2023) 17:38

Page 6 of 14

2.4 Instrumentation and Test Procedures

The axial compression tests were conducted using the CSS-254 universal testing machine of 15 MN loading capacity, as shown in Fig. 4a. The specimens were tested in a displacement-controlled manner at a rate of 0.004 mm/s until failure. The steel plate was placed between the loading plate and the NCS part of the specimens to avoid loading on the UHPC permanent formworks. Only the vertical displacement was constrained during the experiments.

The measurement arrangement of the tested specimens is demonstrated in Fig. 4b. The displacement gauge was mounted onto the loading plate to record the axial deformation. The axial strain of the columns was worked out based on the recorded axial deformation. Additionally, the axial strain was measured by three strain gauges attached to the column surface at mid-height. The measure axial strains were utilized to validate the axial deformation measurement. As shown in Fig. 4b, three horizontal strain gauges were installed at the top, middle, and bottom regions of the column. The axial load was monitored by a load cell of the testing machine. The load, displacement, and strain of the tested columns were recorded by an electronic data acquisition system.

3 Experimental Results and Discussion

3.1 Observed Failure Modes

Since the specimens with the same section showed the same failure modes, the typical failure patterns of each column section are selected and presented in Fig. 5. The NSC columns A, B, and C failure modes were similar. At the initial loading stage, there was no obvious crack in the column specimens. When the axial compression reached around 65% of the ultimate load, the vertical cracks were initiated at the end of the columns. As the loading proceeded, several slight vertical cracks appeared and connected. The connected cracks propagated slowly towards the mid-height region of the column and formed a main long vertical crack with the load increasing. When approaching the ultimate load, the crack reached the middle of the columns, and the concrete at the corner edges began to spall with the crack noise. There was a small lateral deflection caused by the slight accidental eccentricity of the loading apparatus. Finally, the columns reached the ultimate capacity and rapidly failed with the loud sound. The failures of these three types of columns were brittle and followed the typical failure pattern of the long concrete column. As shown in Fig. 5a–c, the concrete of the columns was peeled, and the steel reinforcements were exposed under the peak load.

The initial loading process of the composite column D with the UHPC permanent flat formworks was like the
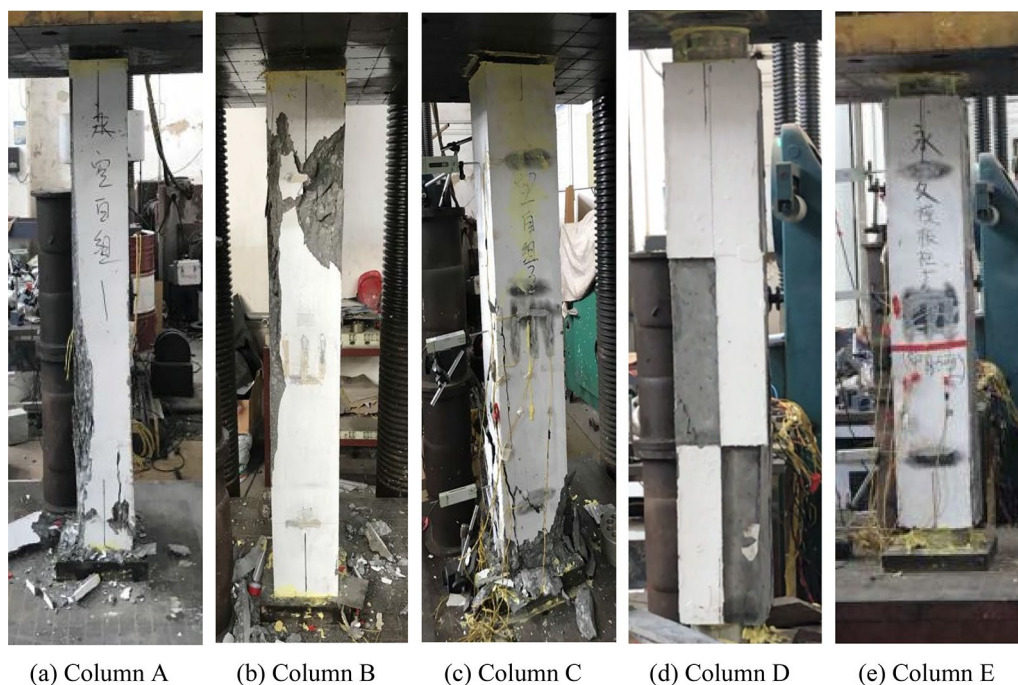

(a) Test apparatus
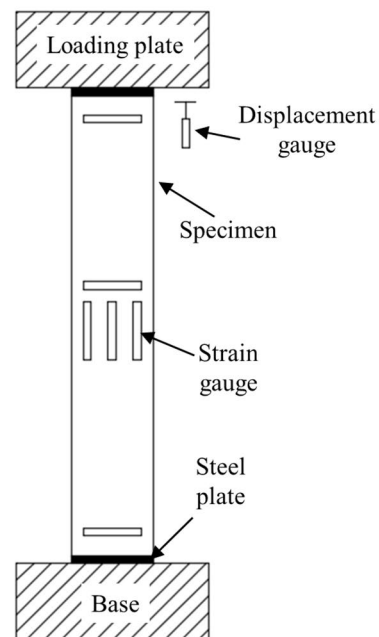
(b) Measurement arrangement

Fig. 4 **a** Test apparatus and **b** schematic diagram of the measurement arrangement

(a) Column A   (b) Column B   (c) Column C   (d) Column D   (e) Column E

Fig. 5 Failure modes of different columns

NSC columns. The initial cracks occurred at the two ends of the column when the axial load reached about 60% of the peak capacity. However, different from the NSC columns, the cracks were mainly in the joints of the UHPC permanent formworks. The slight crack noises could be heard at this stage. With the load rising, the cracks expanded to the middle region along the joints of the formwork systems and formed the vertical straight-line crack across the whole formwork system. When the ultimate load was reached, the inner concrete was crushed with intermittent noises, and the column capacity was lost suddenly. Column D met the brittle failure as well. It can be observed from Fig. 5d that the formworks were peeled from the column due to the expansion of the inner concrete and the straight-line crack between the formworks. After removing the permanent modular formworks and clearing the crushed concrete, the inner part of column D and the peeled formworks are shown in Fig. 6a, b. It can be observed from Fig. 6b that the surface of the formwork was smooth, and the bonding between the inner concrete and the formwork was negligible. The UHPC permanent flat formworks cannot be integrated with the inner concrete effectively.

The failure mode of the composite column E was close to that of the composite column D. However, the ribbed formworks of column E were not peeled under the peak load and were still embedded in the inner concrete. Fig. 6c, d demonstrates the inner concrete and the permanent formworks of the composite column E. It can be noted that a large block of concrete adhered to the formworks, which indicated desirable bonding between the inner concrete and the ribbed permanent formworks. The composite column with ribbed modular formworks possessed better integrity than that with flat modular formworks. This phenomenon was because the ribbed modular formworks have larger contact area with the inner concrete than the flat modular formworks, and the rib could be buried in the inner concrete and provide more interaction with the inner concrete.

3.2 Cracking Load and Ultimate Load

Table 4 summarizes the cracking and ultimate loads of all specimens. The capacities of the different specimens with the same column type had negligible differences, so the average values are discussed in this section. The controlled column A showed superiority over other columns. Due to the increase in the concrete cover thickness, the confinement of the stirrup in column B was not as strong as in column A, which resulted in a decrease in the cracking load and the ultimate loads. The reduction of the cross-section area made the capacity of column C lower than column A. The capacities of the composite columns D and E were significantly lower than the NSC columns B, which meant that the modular UHPC permanent formworks could not offer sufficient confinement and work as the replacement of the concrete cover.
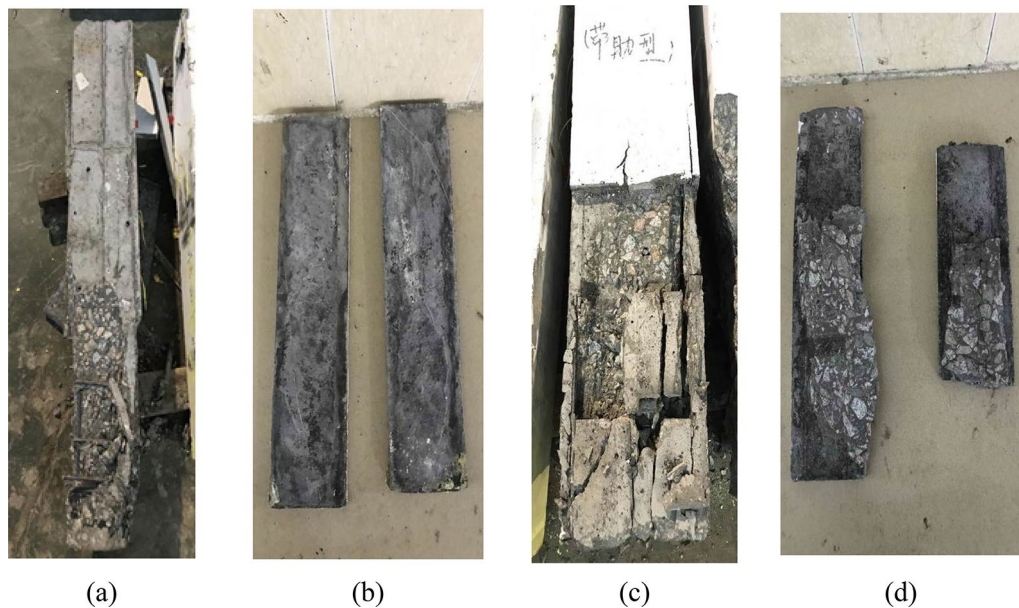
Fig. 6 Failure patterns of the composite columns D and E after removing the UHPC permanent formworks. **a** Inner concrete and **b** removed permanent formwork of the composite column D; **c** Inner concrete and **d** removed permanent formwork of the composite column E

Table 4 The cracking load P_{cr} and ultimate load P_u of specimens

Column type	Specimen	P_{cr} (kN)	P_u (kN)	P_{cr}/P_u (%)	Average P_{cr} (kN)	Average P_u (kN)
A	A-1	1620	2351	68.9	1595	2306
	A-2	1570	2260	69.5		
B	B-1	1390	2218	62.7	1410	2254
	B-2	1430	2290	62.4		
C	C-1	921	1430	64.4	906	1420
	C-2	890	1410	63.1		
D	D-1	780	1352	57.7	760	1321
	D-2	740	1290	57.4		
E	E-1	886	1481	59.8	882	1451
	E-2	878	1420	61.8		

On the other hand, the cracking load and the ultimate load of the composite columns D and E were close to those of the NSC column C, whose section size was the same as the concrete cores of the composite columns D and E. Because of the weakness of the formwork joints, the composite columns D and E cracked earlier than column C. Therefore, it is vital to strengthen the joints of modular formworks in the future. The peeling of the flat formworks made the peak load of column D lower than column C. By comparing column E with column C, it can be noted that the UHPC ribbed permanent formworks could enhance the ultimate strength of column C to some extent. In conclusion, the modular ribbed formworks outperformed the modular flat formworks and could work as the additional cover to the concrete columns with a slight improvement in the ultimate capacity.

3.3 Axial Load–Axial Strain Behavior

Fig. 7 illustrates the typical axial load–axial strain curve of each column type. Due to the limitation of the experimental equipment, the post-failure axial load–axial strain curve was not recorded and presented here. This problem will be addressed by updating the equipment in the future. All types of columns exhibited brittle failure. Prior to the failure, the axial load of all columns ascended almost linearly with the axial deformation. The behaviors of columns close to the linear elastic behavior, and their stiffnesses were close to each other.

Yang *et al. Int J Concr Struct Mater*   (2023) 17:38

Page 9 of 14
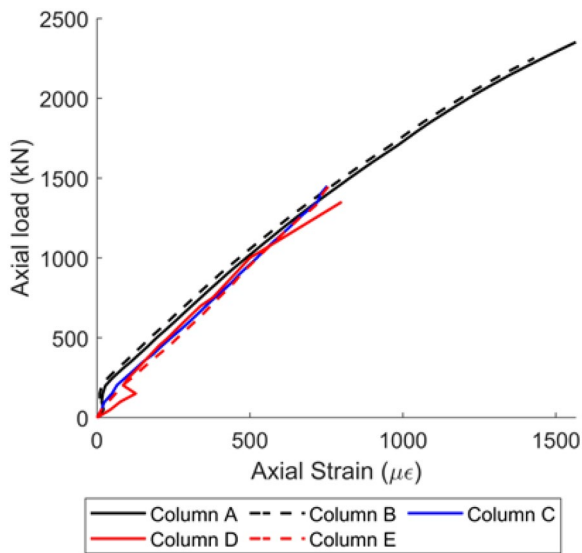
Fig. 7 Axial load–axial strain curves of five types of columns

The sudden loss of strength occurred for all columns after the peak load. The reason of sudden failure was that the yield stress of the steel reinforcement was over 400 MPa, and the concrete of the columns reached its peak strength and crushed suddenly before the steel yielded. In addition, the brittle feature of the UHPC also contributed to the sudden strength loss.
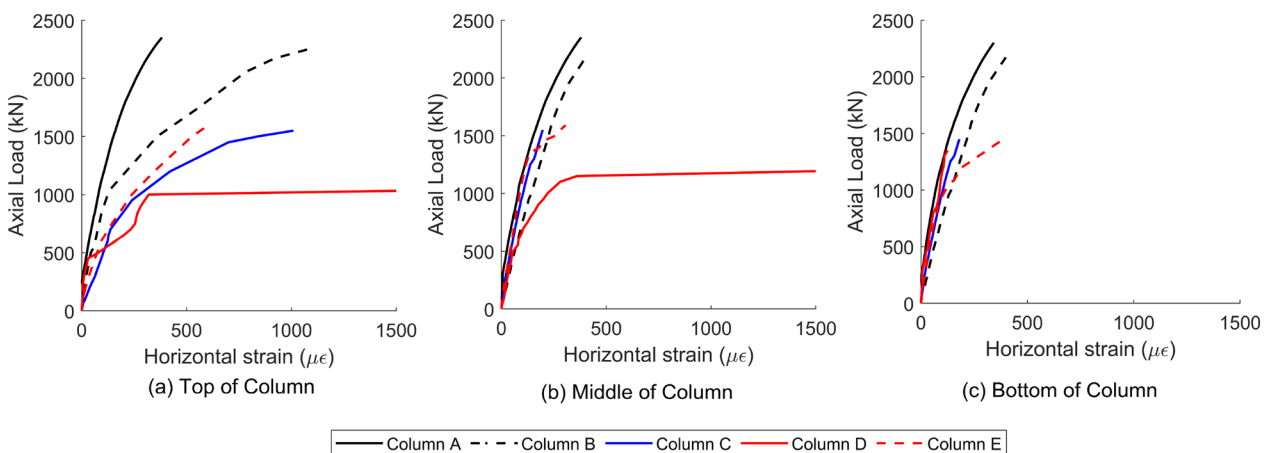
The similar changing trend of the axial load–strain curves was observed by Tian et al. (2020) and Zeng et al. (2022). In their studies Tian et al., (2020) and Zeng et al., (2022), the axial load–strain curves of the reinforced concrete columns fabricated by the one-piece UHPC formworks also presented a first linear elastic ascending portion, and then sharply lost their

strength after the peak load. The consistent failure trend between the modular UHPC formworks proposed in this study and the one-piece UHPC formworks previously investigated by other researchers (Tian et al., 2020; Zeng et al., 2022) evidenced the applicability of the proposed modular formwork. The modular UHPC formwork could also achieve a similar role as the conventional one-piece UHPC formwork.

3.4 Axial Load–Horizontal Strain Behavior

Fig. 8 presents the typical axial load–horizontal strain curves of five column types. The axial loads of columns increased nonlinearly with the horizontal strains. The top of the columns exhibited more significant horizontal strains than the other two parts of the columns. For the top region of the columns, column A showed the slightest horizontal deformation among the three NSC columns, while column C had the most considerable horizontal strain under the same load. Three NSC columns presented a similar ascending trend for the middle and bottom parts of the columns, but column C failed earlier than the other two.

The horizontal strain of column D had the same trend as column C at the initial stage, but its value in the top and middle regions of the column significantly increased when approaching the ultimate load. This dramatic rising was caused by the peeling of the permanent flat formworks. The horizontal deformation performance of the composite column E was close to that of column C as well. The horizontal strains of column E in the middle and bottom regions were slightly larger than those of column C, resulting from the break of the formwork joints. Different from column D, there was no sudden increase in the horizontal strain of column

Fig. 8 Axial load–horizontal strain curves of five types of columns

Yang *et al. Int J Concr Struct Mater* (2023) 17:38

Page 10 of 14

E. It is because the ribbed permanent formworks in the composite column E were effectively integrated with the inner concrete and were not peeled during the loading.

4 Numerical Simulation

4.1 Model Development

In order to further understand the behavior of the composite concrete columns, the finite element analysis (FEA) models of the composite columns D and E, as well as the NSC column C, were established in Midas-FEA software. For the sake of accuracy and efficiency, the tetrahedral elements were used for the NSC column C, and the hexahedron elements were applied for the composite columns D and E. The truss element was used for the reinforcements in all models. The embedded constraint was used between the reinforcements and the concrete. According to the preliminary study, the element size was set to 20 mm. The dimension and boundary conditions were consistent with the experimental conditions. Considering the accidental load eccentricity existing in the experiments, the axial compression was biased 15 mm along the diagonal of the section during the simulation. The established FEA models for three columns are demonstrated in Fig. 9.

Based on the preliminary experimental results, the elastic moduli of the NSC and the UHPC were set to 31,333 MPa and 39,800 MPa, respectively. The Poisson ratios of the NSC and the UHPC were 0.2. The total strain crack model was employed here to describe the constitutive behaviors of the NSC and the UHPC for considering the crack pattern of the concrete columns. The compressive behaviors of the NSC and the UHPC were specified by the Thorenfeldt function with f_c equal to 50.2 MPa and 125 MPa, respectively. The constant tensile function with f_t of 1.57 MPa was used for the NSC, while the linear tensile function with the parameters ($f_t = 10.5$ MPa, $G_f = 1.05$ N/mm, $h = 1.05$ mm) was used for the UHPC. The constant shear retention curve with the β of 0.5 described the shear behavior of both the UHPC and the NSC. The steel reinforcement was described by the von Mises criterion with an elastic modulus of 206,000 MPa and a yield stress of 411.82 MPa.

As observed from the experiments, the bonding between the UHPC flat permanent formworks was weak. Therefore, the interface element with the discrete crack model was generated to separate the NSC core and the UHPC flat formworks. Since the UHPC ribbed permanent formworks were effectively embedded into the inner concrete, the meshes of the UHPC ribbed permanent formworks and the NSC cores were coupled in the FEA model. In addition, the connections between the formworks were modeled by the interface element as well.
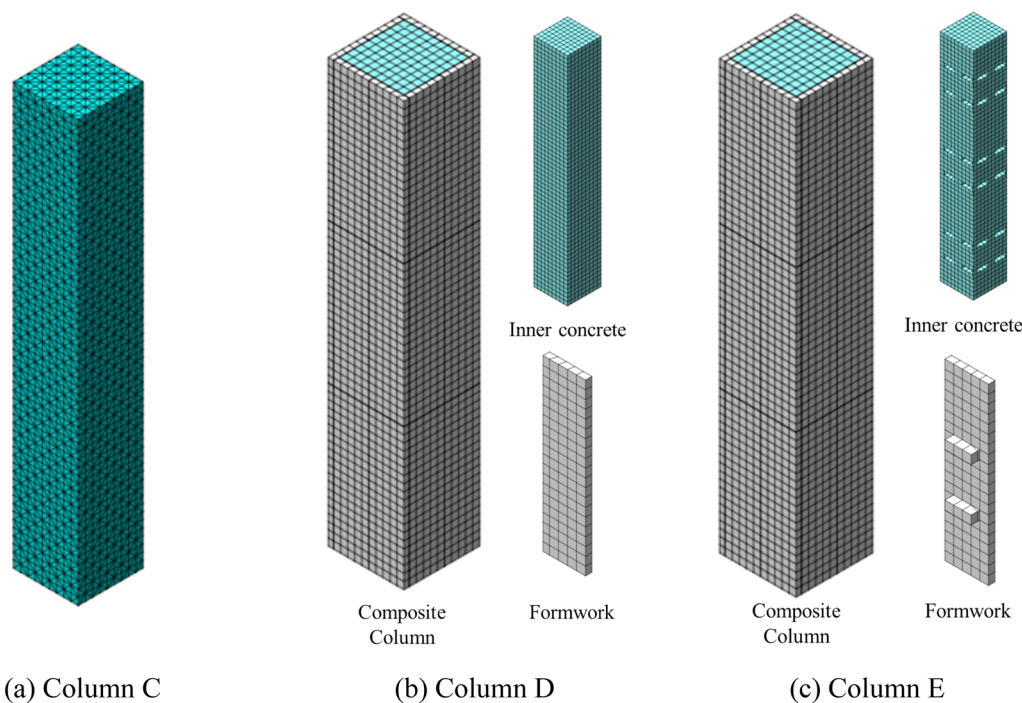

(a) Column C   (b) Column D   (c) Column E

Fig. 9 FEA models of the NSC column C and the composite columns D and E

Table 5 Cracking load P_{cr} and ultimate load P_u given by experiments and numerical simulations

Column type	P_{cr} (kN)		P_u (kN)		
	Experiment	FEA	Experiment	Standard	FEA
C	906	750	1420	1836	1406
D	760	700	1321	–	1450
E	882	750	1451	–	1590

4.2 Results and Discussion

Since the recorded load–strain curves of the column specimens were almost linear, the capacities were directly compared to demonstrate the applicability of the FEA model. The ultimate capacities estimated by the FEA are listed in Table 5, Besides, for the NSC column C, the ultimate capacity calculated by the Chinese standard GB 50010-2010 (2010) is also provided in Table 5. According to the Chinese standard, the ultimate capacity of the concrete column can be estimated by:

$$P_{u-standard} = 0.9\varphi\left(f_y A_s + f_c A\right), \tag{1}$$

where φ is the stability coefficient, f_y is the yield stress of reinforcement, A_s is the cross-sectional area of the reinforcement, f_c is the compressive strength of the NSC, A is the area of the column cross-section. In this case, $\varphi = 1$, $f_y = 400$ MPa, $f_c = 50.2$ MPa, $A_s = 804$ mm^2, $A = 34,225$ mm^2.

The standard value overestimated the load capacity of the NSC column C since the accidental eccentricity of the load was not considered. The ultimate loads predicted by the FEA were generally in good agreement with the tested value, which validated the capacity of the numerical models. The predicted ultimate capacities of the composite beams were slightly larger than the experimental results. This difference can be attributed to the idealization of the formwork joints. The idealized formwork joints were stronger than the actual behaviors, providing the NSC core with more confinement and improving overall capacity.

Fig. 10 shows the von Mises stress distribution of the NCS column C and the concrete cores of the composite columns D and E under the peak load. Due to the eccentric compression, the stress at one edge of column C was larger than at others. It was consistent with the experimental phenomenon that the concrete at the corner edge of the column spalled first under the compression. The confinement of UHPC permanent formworks mitigated this phenomenon to some extent. As observed from Fig. 10b, there was a stress concentration at the position of joints between the flat formworks along the height direction, which contributed to the peeling of the flat formworks during the experiments. For the composite column E, the stress concentration occurred at the embedding position of the ribbed formworks, resulting from the interaction between the ribbed formworks and the inner concrete. The cross-sectional variation of the inner concrete near the embedding position also led to the stress concentration.

With the help of the total strain crack model, the cracking analysis of the concrete columns could be conducted

(a) Column C   (b) Column D   (c) Column E
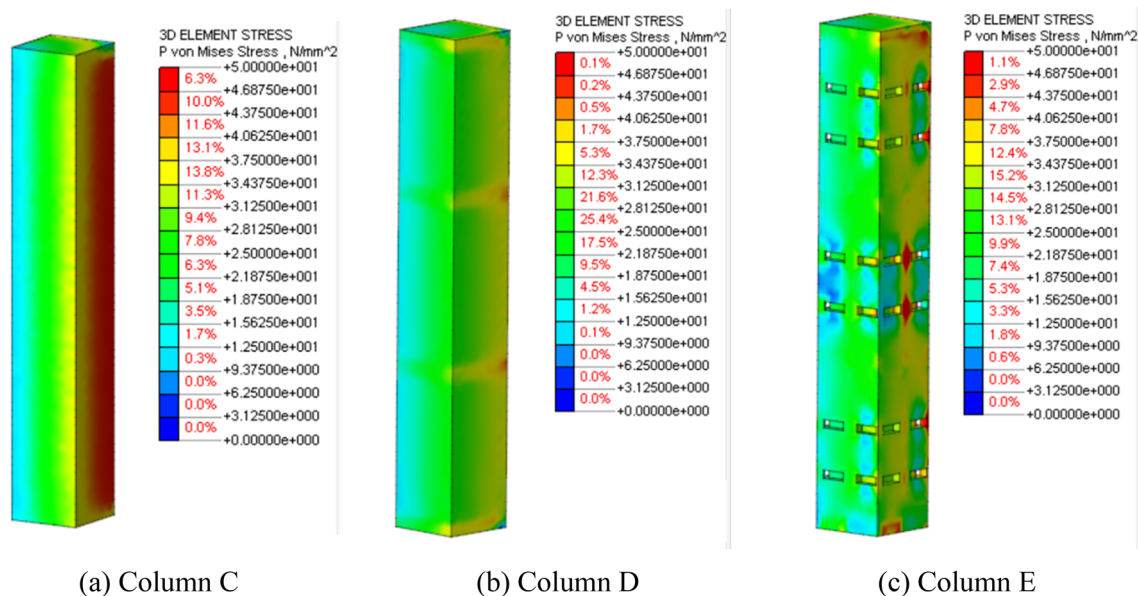
Fig. 10 von Mises stress distribution of **a** NSC column C, **b** concrete core of column D, and **c** concrete core of column E under the ultimate load

by the FEA model. The evaluated cracking loads are presented in Table 5. The predicted cracking loads were smaller than the experimental value, since the experimental values were obtained based on naked-eye observation, and many tiny cracks were not detected. These tiny cracks could be simulated in the FEA models. Because of the limitation of the numerical model and the software, only the crack states at the final stage were visualized in this study. This issue will be solved by applying more advanced numerical crack models in the future. The estimated crack locations and widths under the ultimate loads are illustrated in Fig. 11. Compared with the NSC column C, the composite columns with permanent formworks had more cracks. These cracks were caused by the interaction between the formworks and the inner concrete. The cracks of column D were concentrated around the vertical joints of the flat formworks, which agreed with the experimental observations. For the composite column E, there were many micro-cracks around the embedding position of the ribbed formworks. As the composite column E sustained a larger load than the other two, it also presented more cracks. However, over 90% of the cracks in column E were less than 0.01 mm. Additionally, most of the micro-cracks were located in the inner concrete, so the UHPC permanent formworks could still protect the concrete core from environmental abrasion and improve the overall durability of the composite column.

5 Conclusion

Two modular forms of the ultra-high-performance concrete (UHPC) permanent formwork, namely the flat formwork and the ribbed formwork, were proposed in this work. Both experiments and numerical studies were conducted to investigate the axial compression behaviors of the composite concrete columns encased by two types of UHPC permanent formworks. The comparison between the composite columns and normal strength concrete (NSC) columns was presented as well. The following conclusions were drawn:

(1) The cracks of the composite columns initiated from the modular formwork system's joints and propagated towards the middle of the columns. Similar to the NSC column, brittle failure occurred on the composite columns. Under the ultimate load, the flat formwork was peeled from the concrete core due to the weak bonding, while the ribbed formwork could be desirably embedded into the inner concrete and keep the integrity.

(2) The column encased by the ribbed formwork system exhibited higher load-carrying capacity than the flat formwork one and the NSC column with the same cross-section as the concrete cores of the composite columns. The modular ribbed formworks could be regarded as the additional cover to the NSC column.

(3) The axial load–axial strain behavior and the axial load–horizontal strain behavior of the composite column with the ribbed formworks were close to
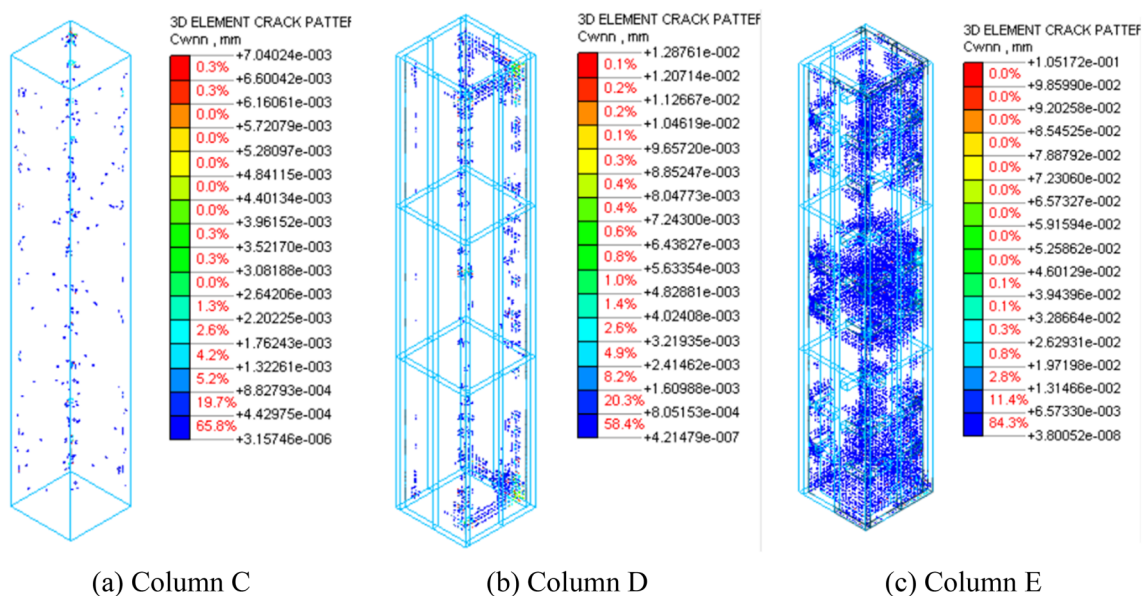

(a) Column C   (b) Column D   (c) Column E

Fig. 11 Numerically estimated cracking patterns of the columns under the ultimate load

Yang *et al. Int J Concr Struct Mater*   (2023) 17:38

Page 13 of 14

the NSC column. Before the peak load, the axial load–axial strain curves presented a linear elastic ascending trend, while the axial load–horizontal strain curves showed a nonlinear rising trend.

(4) As validated by the test results, the finite element analysis (FEA) model exhibited the capacity to simulate the axial compressive behavior of the composite column. The numerical crack analysis illustrated that there were many micro-cracks in the inner NSC concrete of the composite column due to the interaction between the concrete core and the formwork. However, with the protection from the UHPC permanent formworks, the overall durability of the composite column was improved.

Author contributions
YY: methodology, supervision, funding acquisition, writing—review and editing. BC: methodology, investigation, formal analysis, writing—original draft, writing—review and editing. YC: methodology, investigation, data curation. HZ: numerical simulation, investigation. FL: investigation, funding acquisition. XX: investigation, funding acquisition. JC: numerical simulation, investigation. WG: methodology, supervision. HW: methodology, supervision. All authors read and approved the final manuscript.

Authors' information
Yibo Yang is an Associate Professor in School of Civil Engineering and Transportation, South China University of Technology, Guangzhou 510641, China.
Baixi Chen is a Research Associate in Department of Civil and Environmental Engineering, The Hong Kong Polytechnic University, Hung Hom, Kowloon, Hong Kong, China.
Yong Chen is a Postgraduate student in School of Civil Engineering and Transportation, South China University of Technology, Guangzhou 510641, China.
Huangyang Zhou is a Postgraduate student in School of Civil Engineering and Transportation, South China University of Technology is Guangzhou 510641, China.
Fucai Liu is an Engineer in Guangdong Gaiteqi New Materials Technology Co, Ltd, Qingyuan, China.
Xiangming Xie is a Senior Engineer in Guangdong No. 2. Hydropower Engineering Co, Ltd. Guangzhou, China.
Junsheng Chen is an Associate Professor in School of Civil Engineering and Transportation, South China University of Technology, Guangzhou 510641, China.
Wenying Guo is a Lecturer in School of Civil Engineering and Transportation, South China University of Technology, Guangzhou 510641, China.
Hengchang Wang is a Laboratory Technician in School of Civil Engineering and Transportation, South China University of Technology, Guangzhou 510641, China.

Availability of data and materials
The data forming the basis of this study are available from the corresponding authors upon reasonable request.

Declarations

Competing interests
No competing interests exist in the submission of this manuscript.

References
Abed, F., AlHamaydeh, M., & Abdalla, S. (2013). Experimental and numerical investigations of the compressive behavior of concrete filled steel tubes (CFSTs). *Journal of Constructional Steel Research, 80*, 429–439.
Azmee, N. M., & Shafiq, N. (2018). Ultra-high performance concrete: From fundamental to applications. *Case Studies in Construction Materials, 9*, e00197.
Cai, Y., Quach, W.-M., & Young, B. (2019). Experimental and numerical investigation of concrete-filled hot-finished and cold-formed steel elliptical tubular stub columns. *Thin-Walled Structures, 145*, 106437.
Chahrour, A. H., & Soudki, K. A. (2006). RBS polymer encased concrete wall. Part II: Experimental study and theoretical provisions for combined axial compression and flexure. *Construction and Building Materials, 20*(10), 1016–1027.
Fakharifar, M., & Chen, G. (2016). Compressive behavior of FRP-confined concrete-filled PVC tubular columns. *Composite Structures, 141*, 91–109.
Fang, Y., Fang, Z., Feng, L., Xiang, Y., & Zhou, X. (2023). Bond behavior of an ultra-high performance concrete-filled anchorage for carbon fiber-reinforced polymer tendons under static and impact loads. *Engineering Structures, 274*, 115128.
GB/T 14684-2011 Sand for construction, 2011.
GB 50010–2010 Code for design of concrete structure, 2010.
Ghanbari-Ghazijahani, T., Wu, J., & Ng, C.-T. (2020). Plastic buckling and axial crushing of concrete-filled steel tubes: Usage of multiple wood blocks. *Thin-Walled Structures, 150*, 106487.
Graybeal, B., & Tanesi, J. (2007). Durability of an ultrahigh-performance concrete. *Journal of Materials in Civil Engineering, 19*(10), 848–854.
Hadi, M. N. S., Algburi, A. H. M., Sheikh, M. N., & Carrigan, A. T. (2018). Axial and flexural behaviour of circular reinforced concrete columns strengthened with reactive powder concrete jacket and fibre reinforced polymer wrapping. *Construction and Building Materials, 172*, 717–727.
Han, L.-H., Xu, C.-Y., & Tao, Z. (2019). Performance of concrete filled stainless steel tubular (CFSST) columns and joints: Summary of recent research. *Journal of Constructional Steel Research, 152*, 117–131.
Hu, Y.-J., Jiang, C., Liu, W., Yu, Q.-Q., & Zhou, Y.-L. (2018). Degradation of the in-plane shear modulus of structural BFRP laminates due to high temperature. *Sensors, 18*(10), 3361.
Huang, B.-T., Dai, J.-G., Weng, K.-F., Zhu, J., & Shah, S. (2021). Flexural performance of UHPC-concrete-ECC composite member reinforced with perforated steel plates. *Journal of Structural Engineering, 147*, 04021065.
JC/T 1004-2006 Grouts for ceramic wall and floor tiles, 2006.
Jha, K. N. (2012). *Formwork for concrete structures*. Tata McGraw Hill Education private Limited.
Jiang, S., & Shen, L. (2022). Aggregate shape effect on fracture and breakage of cementitious granular materials. *International Journal of Mechanical Sciences, 220*, 107161.
Jiang, S., Shen, L., Guillard, F., & Einav, I. (2021). Characterisation of fracture evolution of a single cemented brittle grain using in-situ X-ray computed tomography. *International Journal of Rock Mechanics and Mining Sciences, 145*, 104835.
Kildashti, K., Samali, B., & Malik, A. (2020). Experimental and numerical studies on the comparison between stay-in-place- and conventionally-formed reinforced concrete columns under concentric loading. *Construction and Building Materials, 258*, 119631.
Kildashti, K., Samali, B., Malik, A., & Alamdari, M. M. (2021). Computational simulation of eccentrically loaded reinforced concrete walls formed with modular thin-walled permanent formwork system. *Journal of Building Engineering, 36*, 102131.
Kuder, K. G., Gupta, R., Harris-Jones, C., Hawksworth, R., Henderson, S., & Whitney, J. (2009). Effect of PVC stay-in-place formwork on mechanical performance of concrete. *Journal of Materials in Civil Engineering, 21*(7), 309–315.
Li, W., Lin, X., Bao, D. W., & Min Xie, Y. (2022b). A review of formwork systems for modern concrete construction. *Structures, 38*, 52–63.

Yang *et al. Int J Concr Struct Mater*   (2023) 17:38

Page 14 of 14

Li, W., Ye, H., Liu, H., & Chen, B. (2022a). Development and testing of demountable RC column-to-steel beam connections under cyclic loading. *Soil Dynamics and Earthquake Engineering, 159*, 107342.

Magureanu, C., Sosa, I., Negrutiu, C., & Heghes, B. (2012) Mechanical properties and durability of ultra-high-performance concrete, *ACI Materials Journal 109*(2).

Ozbakkaloglu, T., & Saatcioglu, M. (2007). Seismic performance of square high-strength concrete columns in FRP stay-in-place formwork. *Journal of Structural Engineering, 133*(1), 44–56.

Remy, O., Verbruggen, S., Wastiels, J., & Tysmans, T. (2011). Cement composite stay-in-place formwork: A concept for future building systems, in *Proceedings of the 18th International Conference on composite materials*

Robert, H. (2007). Think formwork-reduced cost. Structure Magazine, (pp. 14–16).

Shafieifar, M., Farzad, M., & Azizinamini, A. (2017). Experimental and numerical study on mechanical properties of ultra high performance concrete (UHPC). *Construction and Building Materials, 156*, 402–411.

Shan, B., Lai, D.-D., Xiao, Y., & Luo, X.-B. (2018). Experimental research on concrete-filled RPC tubes under axial compression load. *Engineering Structures, 155*, 358–370.

Shan, B., Xu, C., Lai, D. D., Xiao, Y., & Li, T. Y. (2020). Experimental research on compressive behavior of seawater and sea sand concrete-filled RPC tubes. *Engineering Structures, 222*, 111117.

Shi, C., Wu, Z., Xiao, J., Wang, D., Huang, Z., & Fang, Z. (2015). A review on ultra high performance concrete: Part I. Raw materials and mixture design. *Construction and Building Materials, 101*, 741–751.

Tian, H., Zhou, Z., Wei, Y., Wang, Y., & Lu, J. (2019). Experimental investigation on axial compressive behavior of ultra-high performance concrete (UHPC) filled glass FRP tubes. *Construction and Building Materials, 225*, 678–691.

Tian, H., Zhou, Z., Zhang, Y., & Wei, Y. (2020). Axial behavior of reinforced concrete column with ultra-high performance concrete stay-in-place formwork. *Engineering Structures, 210*, 110403.

Wei, Y., Jiang, C., & Wu, Y.-F. (2019). Confinement effectiveness of circular concrete-filled steel tubular columns under axial compression. *Journal of Constructional Steel Research, 158*, 15–27.

Wu, X., Kang, T. H. K., Mpalla, I. B., & Kim, C.-S. (2018). Axial load testing of hybrid concrete columns consisting of UHPFRC tube and normal-strength concrete core. *International Journal of Concrete Structures and Materials, 12*(1), 43.

Xiong, M.-X., & Liew, J. R. (2015). Spalling behavior and residual resistance of fibre reinforced Ultra-High performance concrete after exposure to high temperatures. *Materiales De Construcción, 65*(320), e071–e071.

Yang, Y., Chen, B., Chen, Y., Liu, F., Xie, X., Guo, W., & Wang, H. (2023a). Development of a high strength cementitious grout for filling the joints of UHPC permanent formwork, *Developments in the Built Environment* 100120.

Yang, Y., Chen, B., Chen, Y., Liu, F., Xie, X., Guo, W., & Wang, H. (2023b). Effect of admixtures and PVA fiber on the mechanical properties of high strength cementitious grout, Case Studies in Construction Materials. e01884.

Yang, L., Lin, X., & Gravina, R. J. (2018). Evaluation of dynamic increase factor models for steel fibre reinforced concrete. *Construction and Building Materials, 190*, 632–644.

Yang, Y., Chen, B., Zeng, W., Li, Y., Chen, Q., Guo, W., Wang, H., & Chen, Y. (2021). Utilization of completely recycled fine aggregate for preparation of lightweight concrete partition panels. *International Journal of Concrete Structures and Materials, 15*(1), 1–11.

Ye, H. W., Feng, N. Q., LingHu, Y., Ran, Z. W., Lin, L. X., Qi, S. K., & Dong, Y. (2012). Research on fire resistance of ultra-high-performance concrete. *Advances in Materials Science and Engineering, 2012*, 1–7.

Ying, J., Huang, Y., Qin, L., Gao, X., & Wang, Z. (2021). Axial compressive behavior of GFRP tube confined seawater coral aggregate concrete reinforced with epoxy-coated bars. *Composite Structures, 266*, 113807.

Zeng, J.-J., Chen, S.-P., Peng, K.-D., & Dai, J.-G. (2022). Novel FRP micro-bar reinforced UHPC permanent formwork for circular columns: Concept and compressive behavior. *Composite Structures, 285*, 115268.

Zhang, B., Yu, T., & Teng, J. G. (2015). Behavior of concrete-filled FRP tubes under cyclic axial compression. *Journal of Composites for Construction, 19*(3), 04014060.

Zhang, X., Wu, X., Zhang, D., Huang, Q., & Chen, B. (2022). Axial compressive behaviors of reinforced concrete composite column with precast ultra-high performance concrete (UHPC) jacket. *Journal of Building Engineering, 48*, 103956.

Publisher's Note